Comparison of turbulent premixed flames at different turbulence levels

By Laurent Duchamp de Lageneste AND Heinz Pitsch

1. Introduction

In the flamelet regime, turbulent combustion is characterized by a reaction-zone thickness much smaller than the Kolmogorov length scale (Peters 2000). Thus the internal flame structure remains unaffected by turbulence, and can be approximated by a thin interface separating burnt from unburnt gases.

An equation describing the dynamics of such a surface has been presented in Williams (1985) and is now known as the G-equation. It is based on the flamelet assumption and uses the general level-set methodology described in detail in Sethian (1996) and Osher & Fedkiw (2002). Variants of this model have been used in conjunction with Reynolds-averaged Navier-Stokes models (RANS) (Peters 2000; Herrmann 2000) or large-eddy simulation models (LES) (Smith & Menon 1997; Kim & Menon 2000; Chakravarthy & Menon 2000; Sankaran & Menon 2000; Duchamp de Lageneste & Pitsch 2001).

Pitsch & Duchamp de Lageneste (2002) have formulated a level-set method based on the G-equation for LES of premixed turbulent combustion in which a specific filtering procedure respecting the particular symmetries of the G-equation (Oberlack *et al.* 2001) has been used.

As a validation of the model and to demonstrate the benefits of LES in turbulent combustion modeling, we report in the present paper on the LES of two Bunsen flames, the F3-flame and the F2-flame from the series of experiments by Chen *et al.* (1996). These flames are nominally in the regime of thin reaction zones (Peters 2000) but F2, which has a higher turbulence level and hence a higher Karlovitz number, is closer to the regime of distributed reaction zones than F3.

After briefly recalling the main equations used in the level-set modeling of premixed turbulent combustion, we will compare results from the simulations to the experimental data of Chen *et al.* (1996). As a first step, results from the cold-flow simulations will be presented to ensure that adequate boundary conditions are used in the LES. This cold flow will also be used as a validation of the flow solver as well as a reference computation, to be used later to assess the ability of the LES to capture flow changes due to combustion.

We will then present and discuss results concerning the reacting cases, where time-averaged quantities such as axial velocity, turbulent kinetic energy and temperature will be compared to the data of Chen *et al.* (1996).

2. Level-set method

We briefly recall here the main equations and models involved in the level-set LES of premixed turbulent combustion. The derivation and discretization of this method is discussed in detail in previous reports. In the following equations, all symbols denote filtered quantities unless otherwise noted.

The level-set equation (or G-equation) for LES is written as:

$$\frac{\partial G}{\partial t} + \mathbf{U} \cdot \nabla G = \frac{\rho_u}{\rho} \left(s_T - D_t \kappa \right) |\nabla G| \,, \tag{2.1}$$

where $\mathbf{U}$ is the convection velocity, s_T the turbulent burning velocity, ρ_u the unburnt density, and κ the curvature.

An algebraic model similar to the one derived for RANS by Peters (2000) is used for the turbulent burning velocity:

$$\frac{s_T - s_L}{s_L} = -\frac{C_\nu b_3^2}{2 b_1 Sc_{t,G}} \frac{\Delta}{l_F} + \left[\left(\frac{C_\nu b_3^2}{2 b_1 Sc_{t,G}} \right)^2 + \frac{b_3^2 D_t}{s_L l_F} \right]^{\frac{1}{2}} \,, \tag{2.2}$$

where Δ is the filter width, $D_t = C_\nu \Delta v'_\Delta / Sc_{t,G}$ the turbulent diffusivity computed with a constant turbulent Schmidt number of $Sc_{t,G} = 0.5$ according to Pitsch & Steiner (2000), v'_Δ being the turbulent velocity fluctuation, and s_L and l_F the laminar burning velocity and flame thickness respectively. The constants b_1 and b_3 are evaluated by Peters (2000) as $b_1 = 2.0$ and $b_3 = 1.0$.

In the case where dilution or partial-premixing effects are to be considered, an equation for the conserved mixture fraction Z is also solved together with an equation for the reduced temperature $\theta = (T - T_u)/(T_b - T_u)$. If heat losses are included in the model, an equation for the enthalpy H is also used. These equations are:

$$\rho \frac{\partial Z}{\partial t} + \rho \mathbf{U} \cdot \nabla Z = \nabla \cdot \left(\rho D_t^Z \nabla Z \right) , \tag{2.3}$$

$$\rho \frac{\partial \theta}{\partial t} + \rho \mathbf{U} \cdot \nabla \theta = \nabla \cdot \left(\rho D_t^\theta \nabla \theta \right) + \rho \omega \,, \tag{2.4}$$

and:

$$\rho \frac{\partial H}{\partial t} + \rho \mathbf{U} \cdot \nabla H = \nabla \cdot \left(\rho D_t^H \nabla H \right) . \tag{2.5}$$

On the burnt side, the temperature is given as a function of Z and its subgrid variance by pre-computing a laminar flamelet library similar to the one classically used in non-premixed combustion (Peters 2000). Although, since an equation for the temperature is already solved, it may seems redundant to use an extra equation for the enthalpy, H is used only as a parameter in the generation of the flamelet library to take possible heat losses into account. On the unburnt side, the temperature is simply given by the solution of (2.4). Hence, (2.4) is really only solved in the unburnt region, with the burnt temperature evaluated from the flamelet library acting as a boundary condition at the flame surface.

In order to distinguish between burnt and unburnt regions, the probability of burning $P_b = P_{G \geq G_0}$ is defined using an assumed PDF approach. Assuming a Gaussian sub-filter distribution for G, this PDF is given by:

$$P_{G \geq G_0} = \int_{\xi = G_0}^{\infty} \frac{1}{\sqrt{2\pi G''^2}} exp \left[-\frac{(G - \xi)^2}{2 G''^2} \right] d\xi \,. \tag{2.6}$$

The filtered source term appearing in (2.4) is expressed as: $\omega = P_b(\theta - \theta_{flamelet})$, thus setting the temperature to the value prescribed by the flamelet library ($\theta_{flamelet}$) on the burnt side while vanishing on the unburnt side.

All subgrid quantities such as the subgrid variances Z''^2 and G''^2 or the turbulent

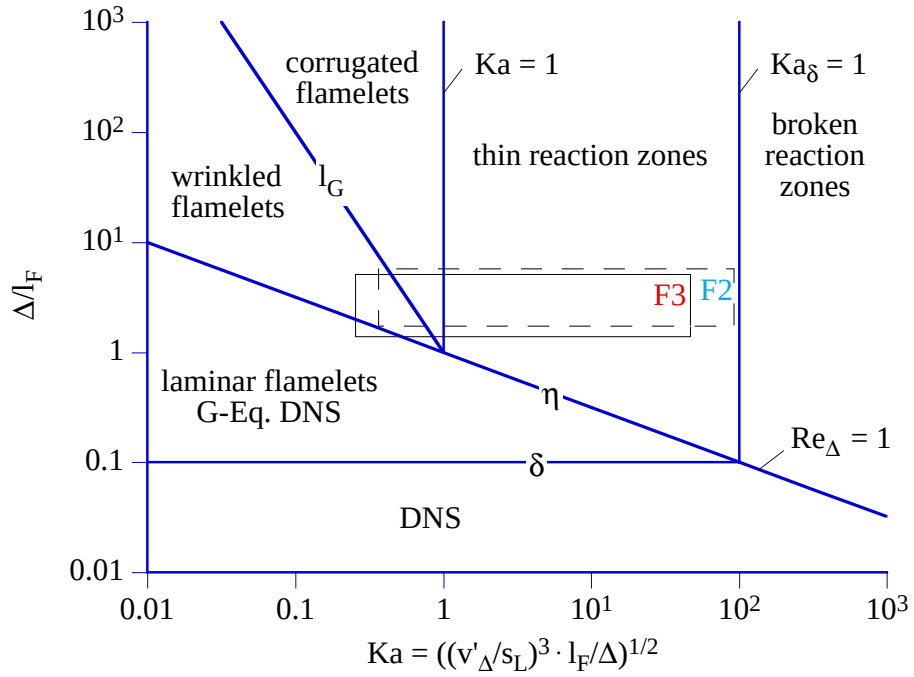

FIGURE 1. LES regime diagram. The non-dimensional filter width is plotted as a function of the Karlovitz number. The areas covered by the values of the parameters computed along an instantaneous flame surface for F2 and F3 are shown as rectangles.

diffusivities $D_t^{\theta,H,Z}$ are computed using the dynamic approach developed by Moin *et al.* (1991) and Pierce & Moin (1998).

3. Numerical simulation

3.1. *Experimental setup*

Flame F2 and F3 are turbulent Bunsen flames, studied experimentally by Chen *et al.* (1996). The experimental setup is the same in both cases, and consists of an axial-symmetric central jet of diameter $D = 12\,\mathrm{mm}$ surrounded by a large pilot flame. A stoichiometric mixture of methane and air is used for the central jet as well as the pilot flame. The whole apparatus is surrounded by air at rest.

The mean exit velocity of the central jet is different in each case, with $U_0 = 50\,\mathrm{m/s}$ for F2 and $U_0 = 30\,\mathrm{m/s}$ for F3. Experimental data are available for the cold flow as well as the reacting flow at different downstream stations.

Chen *et al.* (1996) have shown that both flames are mainly in the regime of thin reaction zones. This is confirmed by showing in figure 1 the values of the non-dimensional filter width and corresponding Karlovitz number computed along an instantaneous flame surface for F2 and F3. The rectangles in figure 1 are used to represent the area covered by the parameter values in both cases, and F2 is shown to have on average a higher Karlovitz number than F3.

3.2. *Grid and boundary conditions*

We use the structured code developed at CTR by Pierce & Moin (2001), in which the low-Mach-number approximation to the Navier-Stokes equations is solved using a second-order finite-volume scheme on a staggered cylindrical grid.

The computational domain extends $20D$ downstream of the nozzle and $4D$ in the radial direction. The grid of $256\times96\times64$ nodes corresponds to approximately 1.6 million cells, and is refined around the wall separating the central jet from the pilot in the radial direction.

Convective boundary conditions (Akselvoll 1996) are prescribed at the outlet, while instantaneous profiles, obtained from a separate, fully-developed turbulent pipe flow LES, are prescribed at the central jet inlet. The surrounding pilot is considered to be a laminar inflow with a prescribed mean velocity, computed using the mean mass-flow rate given in the experiment.

Before discussing the results, a few remarks concerning the experimental results and their subsequent consequences on our modeling assumptions are worth making:

- In the experiment, the pilot nozzle consists of an array off small jets issued through a cooled perforated plate (1175 holes of 1 mm in diameter), forming a flat flame above the plate's surface. This configuration leads to heat losses at the plate surface which are modeled in the simulation by choosing an appropriate enthalpy for the fluid issuing from the pilot to give the correct temperature distribution at the first measurement station downstream of the nozzle, which is located at $x/D = 0.25$.
- While the inlet profiles used in the simulation of the central jet are those of a fully developed pipe flow, experimental data close to the inlet section show that the flow may not be fully developed. Nevertheless, it will be shown that these differences are small and are unimportant further downstream.
- Since the only difference between F2 and F3 is the mean velocity of the central jet, the only parameter that has been changed in our simulations is the Reynolds number.

4. Results and discussion

In this section we present some comparisons between the results from the LES and the experimental data reported by Chen *et al.* (1996). In particular, we discuss predictions of mean quantities such as mean axial velocity or temperature, as well as turbulent quantities like the turbulent kinetic energy and turbulent flame-brush thickness.

We first focus briefly on cold-flow results before presenting a more detailed study of reacting-flow simulations.

4.1. *Cold flow*

In this section, we compare some of the LES results for the non-reacting flows with corresponding experimental data. The purpose of this comparison is twofold:

- It serves as a validation of the flow solver, insuring that grid and boundary conditions are properly chosen,
- By comparing the cold-flow results with reacting-flow results presented below, the data will be used to assess the ability of the LES to capture flow changes generated by the combustion process.

4.1.1. *Mean axial velocity*

Figure 2 shows a comparison between computed (solid lines) and measured (symbols) radial profiles of mean axial velocity at two downstream locations. As expected, the

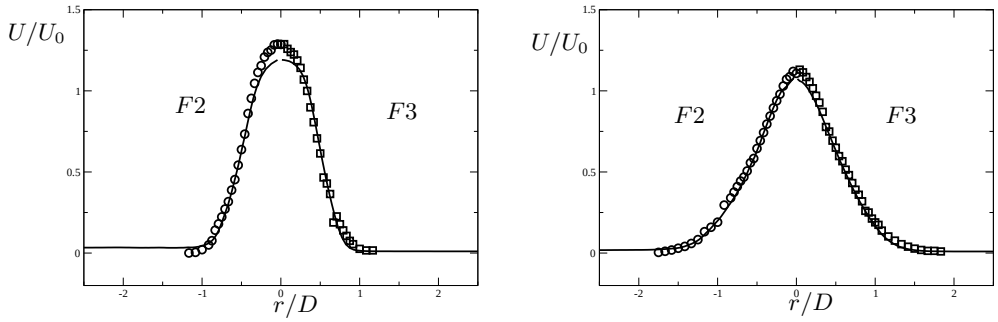

FIGURE 2. Cold flow. Radial profiles of mean axial velocity. Solid lines denote the LES results, symbols denote experimental data. Stations: $x/D = 2.5$ (left) and $x/D = 6.5$ (right).

experimental data shows the spreading of the jet corresponding to the development of the lateral shear layers. The end of the potential core is observed at roughly $x/D = 4.5$, and the maximum mean velocity decreases from thereon as the jet expands in the radial direction.

The LES captures these effects very accurately. Some discrepancies in the maximum jet velocity can be seen at the first station and indicate that our assumption of a fully developed pipe flow at the inflow may not have been fully realized in the experiment. Nevertheless, these small discrepancies vanish further downstream and do not seem to affect the accuracy of the results.

With proper non-dimensionalization, very little difference can be observed between F2 and F3, underlining the self-similar development of the jets.

Overall, the agreement between the LES and the experimental data is very good.

4.1.2. *Turbulent kinetic energy*

Figure 3 shows radial profiles of turbulent kinetic energy for the same downstream locations as in the previous section. These profiles also show the radial spreading of the lateral shear layers surrounding the central jet and it can be seen that radial mixing increases, both outwards and inwards, with distance from the nozzle. In particular, the increase of turbulent kinetic energy close to the centerline indicates the merging of the lateral shear layers and thus the end of the potential core. It is to be noted that the peak turbulent kinetic energy is constant up to $x/D = 6.5$ and that, again, no significant differences can be observed between F2 and F3.

The results extracted from the LES capture the downstream evolution of the turbulent kinetic energy with very good accuracy.

4.2. *Reacting flow*

In this section, results from the LES of flames F2 and F3 are compared to experimental data from Chen *et al.* (1996). Comparisons are shown between cold and reacting flows, but also between the two reacting flows, to assess the ability of the LES to predict not only the impact of combustion on the flow field but also the changes with Reynolds number.

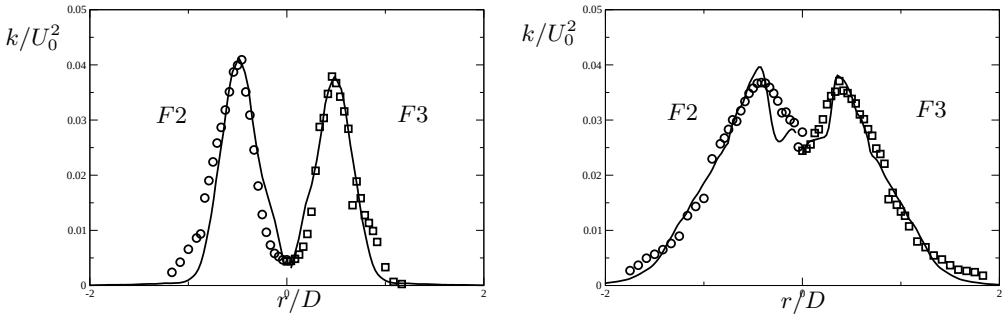

FIGURE 3. Cold flow. Radial profiles of turbulent kinetic energy. Solid lines denote the LES results, symbols denote experimental data. Stations: $x/D = 2.5$ (left) and $x/D = 6.5$ (right).

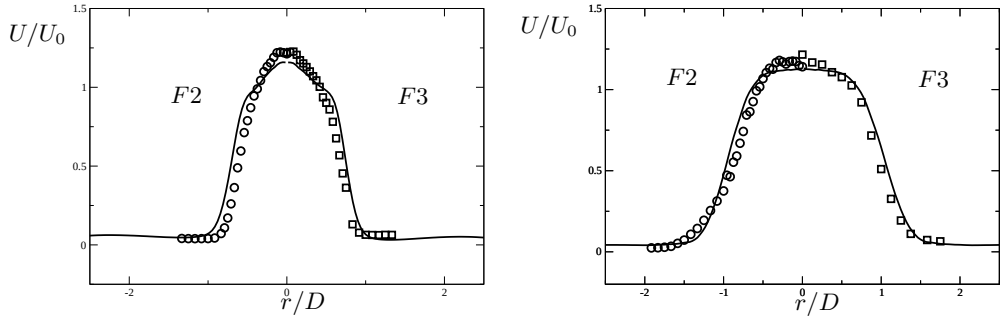

FIGURE 4. Reacting flow. Radial profiles of mean axial velocity. Solid lines denote the LES results, symbols denote experimental data. Stations: $x/D = 2.5$ (left) and $x/D = 6.5$ (right).

4.2.1. *Mean axial velocity*

Figure 4 shows radial profiles of the mean axial velocity at the two downstream stations $x/D = 2.5$ and $x/D = 6.5$. Results for flame F2 are on the left side while those for F3 are on the right. Symbols represent experimental data, solid lines the numerical results.

A first interesting comparison can be made between figure 4 and figure 2 concerning the ability of the LES to capture the effect of heat release on the mean flow pattern. In this respect, the experimental data show that the presence of combustion has qualitatively the same effect on the mean velocity profiles for both flames:

- radial profiles are broadened because of the divergence of the mean streamlines due to gas expansion,
- the maximum velocity observed around the centerline stays approximately constant up to the axial position where the fuel is almost completely consumed, showing an extension of the potential core in the reacting case.

These significant differences between cold and reacting cases are particularly apparent if one compares figure 4 to figure 2 for the downstream station $x/D = 6.5$. It can also be seen in these figures that the LES reproduces these effects accurately.

We will now focus on the specific differences between the two reacting cases. The main

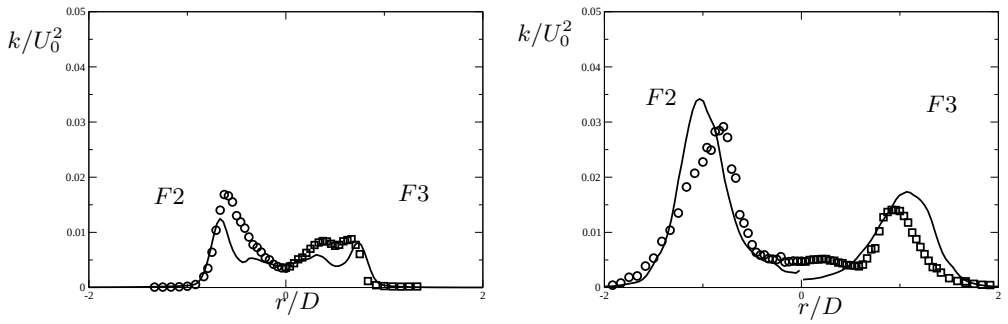

FIGURE 5. Reacting flow. Radial profiles of turbulent kinetic energy. Solid lines denote the LES results, symbols denote experimental data. Stations: $x/D = 2.5$ (left) and $x/D = 6.5$ (right).

difference from the experimental data is the apparent larger broadening of the axial velocity profile in the F3 case compared with F2. This phenomenon can be observed at both stations and is well predicted by the simulation. It is consistent with the lower jet exit velocity for F3, leading to a relatively faster flame. F3 being shorter than F2, its angle with the burner is smaller and leads to a wider spreading of the jet.

The overall quantitative agreement between computation and experiment is good, although one can observe in figure 4 a slight overprediction of the jet spreading rate in both cases. An explanation for this discrepancy will be given in section 4.2.3.

4.2.2. *Turbulent kinetic energy*

Figure 5 displays radial profiles of turbulent kinetic energy at stations $x/D = 2.5$ and 6.5 and can be compared to figure 3. Large differences can be observed between the cold and the reacting cases.

First, the turbulent fluctuations are greatly reduced in the reacting case due to the increased viscosity and the dilatation caused by the heat release. This is especially apparent at $x/D = 2.5$, where the peak intensity was found experimentally to be reduced by 58% for F2 and 75% for F3 compared to the cold case. This trend is well reproduced by the simulation although to a slightly higher extent as reductions of 66% and 77% are observed for F2 and F3 respectively.

Furthermore, computational and experimental results shown in figure 3 show an increasing turbulent kinetic energy close to the centerline for the cold case, but figure 5 shows relatively constant levels for both reacting cases. This indicates that the shear layer surrounding the jet are deflected outward in the reacting cases due to heat release, extending the potential core up to the axial position where most of the fuel is consumed, and therefore prevents radial mixing.

In addition, it was noted in section 4.1.2 that turbulent kinetic energy levels for the cold cases were relatively constant up to $x/D = 6.5$. In contrast, the peak intensity computed in the LES increases in the downstream direction for both reacting cases, and follows the trend observed experimentally, levels for F2 are always higher than for F3.

It was also reported in section 4.1.2 that no significant difference could be found between the F2 and F3 turbulent kinetic energy profiles for the cold cases, whereas results and experimental data show large qualitative and quantitative differences for the reacting cases. For instance, at the first station $x/D = 2.5$, the experimental results for F3 show

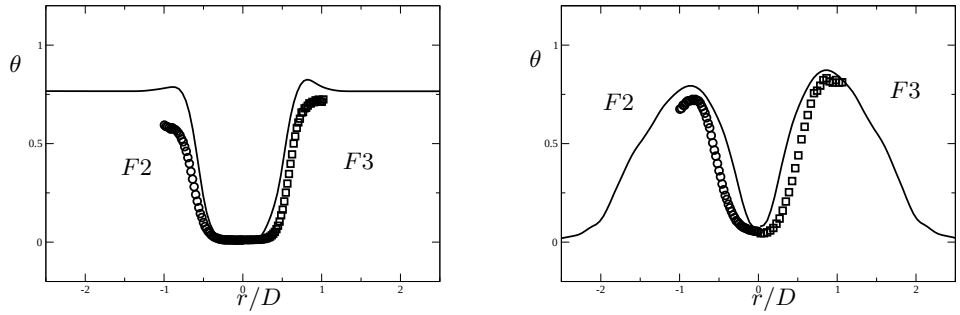

FIGURE 6. Reacting flow. Radial profiles of reduced mean temperature. Solid lines – LES results, symbols – experimental data. Stations: $x/D = 2.5$ (left) and $x/D = 6.5$ (right).

that the radial profile exhibits two peaks. The first one, located on the burnt side of the flame, is also observed in the F2 results and increases along the streamwise direction whereas the second one, found on the unburnt side, is not observed for F2, and vanishes further downstream. This particular behavior is qualitatively well predicted by the LES as shown in figure 5.

While the overall quantitative predictions from the LES are reasonable, figure 5 shows that the LES slightly underpredicts turbulent kinetic energy levels at $x/D = 2.5$ while it overpredicts this same quantity at $x/D = 6.5$, this trend can be observed for both F2 and F3.

4.2.3. *Mean temperature*

Figure 6 shows the radial profiles of the mean reduced temperature defined by

$$\theta = \frac{T - T_u}{T_b - T_u}\,, \tag{4.1}$$

where T_u is the unburnt temperature and T_b the burnt temperature.

At $x/D = 2.5$, the most important difference between F2 and F3 reported by Chen *et al.* (1996) is the considerably lower mean temperature observed for flame F2. Whereas flame F3 is already found to be at a reduced temperature approximately 25 % lower than the adiabatic flame temperature due to heat losses at the burner surface, F2 temperature is even lower (about 45 %). This difference can be explained by the combined effect of heat losses at the burner exit and increased fluctuations of the flame front.

As shown in figure 6, LES results for F3 are overpredictions, but still reasonable with a maximum discrepancy around 10 % whereas those for F2 show a maximum discrepancy of around 25 %. This tendency of the LES to overpredict the mean temperature is consistent with the overprediction of the jet spreading rate noted in section 4.2.1, as well as with the lower predicted turbulence intensities observed at $x/D = 2.5$ (section 4.2.2). However, it is observed in figure (6 that the predictions tend to become better further downstream, such that results at $x/D = 6.5$ are in reasonable agreement with experimental data. Thus, the major discrepancies observed between our simulations and the experimental data of Chen *et al.* (1996) are found to be confined to the first few diameters downstream of the jet exit.

Since heat losses at the burner exit are taken into account in both simulations and are

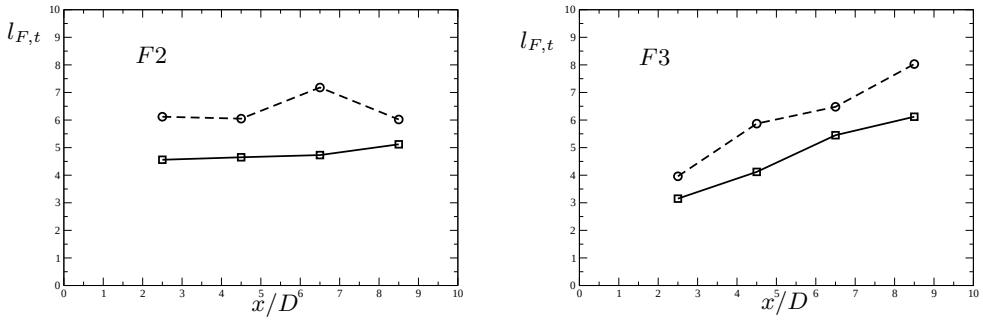

FIGURE 7. Downstream evolution of the mean turbulent flame-brush thickness $l_{F,t}$. Solid lines denotes LES, dashed lines experimental results. F2 flame (left) and F3 flame (right).

not expected to be very different from F3 to F2, we will now focus on the predictions of the flame front fluctuations.

4.2.4. *Turbulent flame-brush thickness*

In Chen *et al.* (1996), the turbulent flame-brush thickness is defined as a measure of the flame-front fluctuations and is computed as

$$l_{F,t} = \left[\frac{\partial\overline{\theta}}{\partial r}\right]^{-1}_{\max} . \tag{4.2}$$

Figure 7 shows the values of $l_{F,t}$ extracted from the experimental data of Chen *et al.* (1996) at four different downstream stations $x/D = 2.5$, $x/D = 4.5$, $x/D = 6.5$ and $x/D = 8.5$ for flames F2 and F3 compared with the corresponding values obtained from the LES.

It is immediately apparent that the LES underpredicts the turbulent flame-brush thickness at every station for both flames. If one considers only the results for the first station $x/D = 2.5$, it is seen that the experiment predicts an increase of the turbulent flame brush of nearly 60% when going from F3 to F2, whereas the LES shows an increase closer to 45 %. Thus LES underpredicts the turbulent flame-brush thickness of flame F2 by almost 30 %, which could explain the overprediction of the mean temperature at $x/D = 2.5$. A possible reason for this systematic underprediction of the flame-surface wrinkling could be the presence of a curvature term in (2.1). This term tends to damp any small instability occurring at the flame front. Pitsch (2002) presents a new derivation of the G-equation for LES where this curvature term does not appear. Further validation of this new formulation with the F2 and F3 cases will assess the impact of the curvature on the flame-front wrinkling and is in progress.

On a more qualitative level, the results shown in figure 7 also show significant differences in the downstream evolution of l_F for F2 and F3. While $l_{F,t}$ increases linearly with distance from the burner for F3, it seems to stay constant for F2. This behavior is also observed in the LES, and can be linked to the higher Reynolds number of flame F2.

5. Conclusions

This paper presents results from the LES of two turbulent Bunsen flames at different Reynolds and Karlovitz numbers. A level-set method has been used as a model for turbulent premixed combustion and comparison are made with the experimental data of Chen *et al.* (1996). As a validation of the flow solver, computations of the corresponding cold cases have been carried out and used as references to assess the ability of the LES to predict the changes of the flow patterns due to combustion.

From the cold-flow simulations, it has been shown that inflow and boundary conditions are properly chosen, and that the flow solver predicts results in very good agreement with experimental data.

Subsequent comparisons of the reacting-flow characteristics have shown that the level-set approach is able to reproduce the main characteristics of the turbulent flames studied. In particular, the changes in the mean flow pattern due to heat release, such as the increased spreading of the jet and decreased turbulent kinetic energy, are well captured. Furthermore, the main flow differences between F3 and F2, such as the higher spreading rate and lower turbulent kinetic energy of F3 compared with F2, are reasonably well reproduced by the LES.

Nevertheless, mean temperature profiles were shown to be overpredicted in the first few diameters downstream of the nozzle, especially for F2. These discrepancies were traced to an underprediction of the turbulent fluctuations of the flame front and a possible link with the presence of a curvature term in the G-equation was suggested.

Acknowledgments

The authors gratefully acknowledge funding by the US Department of Energy within the ASCI program, and by SNECMA Moteurs.

REFERENCES

Akselvoll, K. 1996 An efficient method for temporal integration of the navier-stokes equations in confined axisymmetric geometrie. *J. Comp. Phys.* **125**, 454–463.

Chakravarthy, V. K. & Menon, S. 2000 Subgrid modeling of turbulent premixed flames in the flamelet regime. *Flow, Turb. and Comb.* **5**, 23–45.

Chen, Y. C., Peters, N., Schneemann, G. A., Wruck, N., Renz, U. & Mansour, M. S. 1996 The detailed flame structure of highly stretched turbulent premixed methane-air flames. *Comb. and Flame* **107**, 233–244.

Herrmann, M. 2000 Numerische simulation vorgemischter und teilweise vorgemischter turbulenten flammen. PhD thesis, RWTH, Aachen.

Kim, W. W. & Menon, S. 2000 Numerical modeling of turbulent premixed flames in the thin-reaction zones regime. *Comb. Sci. Tech.* **172**, 1–32.

Duchamp de Lageneste, L. & Pitsch, H. 2001 Progress in large-eddy simulation of premixed and partially-premixed turbulent combustion. In *Annual Research Briefs*, Center for Turbulence Research, NASA Ames/Stanford Univ., pp. 97–107.

Moin, P., Squires, K., Cabot, W. & Lee, S. 1991 A dynamic subgrid-scale model for compressible turbulence and scalar transport. *Phys. Fluids* **A**, 2746–2757.

Oberlack, M., Wenzel, H. & peters, N. 2001 On symmetries and averaging of the G-equation for premixed combustion. *Comb. Theo. and Model.* **5**, 1–20.

Osher, S. & Fedkiw, R. 2002 *Level set methods and dynamic implicit surfaces*, *Applied Mathematical Sciences*, vol. 153. Springer, New York.

Peters, N. 2000 *Turbulent Combustion*. Cambridge University Pres.

Pierce, C. D. & Moin, P. 1998 Large eddy simulation of a confined jet with swirl and heat release. *AIAA Paper* 98-2892.

Pierce, C. D. & Moin, P. 2001 Progress-variable approach for large eddy simulation of turbulent combustion. *Tech. Rept.* TF-80. Dept. Mech. Engg., Stanford University.

Pitsch, H. 2002 A G-equation formulation for large-eddy simulation of premixed turbulent combustion. In *Ann. Research Briefs*, Center for Turbulence Research, NASA Ames/Stanford Univ.,

Pitsch, H. & Duchamp de Lageneste, L. 2002 Large-eddy simulation of premixed turbulent combustion using a level-set approach. In *Proceedings of the* 29^{rd} *Symposium on Combustion*. The Combustion Institute. Accepted for publication.

Pitsch, H. & Steiner, H. 2000 Large eddy simulation of a turbulent piloted methane/air diffusion flame. *Phys. Fluids* **12** (10), 2541–2553.

Sankaran, V. & Menon, S. 2000 Structure of premixed flame in the thin-reaction zones regime. In *Proceedings of the* 28^{th} *Symposium on Combustion*. The Combustion Institute, Pittsburg, pp.123–129.

Sethian, J. A. 1996 *Level Set Methods : Evolving Interfaces in Geometry, Fluid Mechanics, Computer Vision and Material Science*. Cambridge University Press.

Smith, T. M. & Menon, S. 1997 One-dimensional simulations of freely propagating turbulent premixed flames. *Comb. Sci. Tech.* **128**, 99–130.

Williams, F. A. 1985 Turbulent combustion. In *Math. of Comb.* (Frontiers in Applied Mathematics, vol 2, J. Buckmaster, ed.) SIAM, Philadelphia